NANO LETTERS

pubs.acs.org/NanoLett

Visualizing the Optical Interaction Tensor of a Gold Nanoparticle Pair

Bradley Deutsch,[†] Rainer Hillenbrand,[‡,§] and Lukas Novotny*[,†]

[†]Institute of Optics, University of Rochester, Rochester, New York 14627, [‡]Nanooptics Laboratory, CIC nanoGUNE Consolider, 20018 Donostia — San Sebastián, Spain, and [§]IKERBASQUE, Basque Foundation for Science, 48011 Bilbao, Spain

ABSTRACT The control of optical fields on the nanometer scale is a central theme of plasmonics and nanophotonics. Methods for characterizing localized optical field distributions are necessary to validate theoretical predictions, to test nanofabrication procedures, and to provide feedback for design improvements. Typical methods of probing near fields (e.g., single molecule fluorescence and near-field microscopy) cannot probe both the complex-valued and vectorial nature of the field distributions. We demonstrate that a nanoparticle probe with isotropic polarizability in combination with polarization control of excitation and detection beams provides access to this information through the interaction tensor. For a sample consisting of a single nanoparticle we show that the recorded images correspond to maps of the local Green's function tensor elements that couple the probe and sample. The tensorial mapping of interacting nanoparticles is of interest for optical sensing, optical antennas, surface-enhanced Raman scattering, nonlinear optics, and molecular rulers.

KEYWORDS Near-field optical imaging, nanoplasmonics, optical antennas, inverse scattering, nanoparticles

The mapping of optical near fields is of central importance for problems in plasmonics and nanophotonics. The optical near field is generally more complicated than the optical farfield because of stronger spatial variations, the possibility of coherence lengths smaller than half the wavelength,[1] and three-dimensional polarization states.[2,3] A general polarization state at a point in space can be represented by a complex vector that traces out an ellipse.[4] To characterize this ellipse, a measurement must be sensitive to the vector's direction,[5] as well as its magnitude and phase.

Optical near fields are most commonly characterized by single-molecule fluorescence detection[6,7] or by near-field optical microscopy.[4,5,8−16] In single-molecule experiments the local electric field $\mathbf{E}$ is projected on the dipole axis $\mathbf{p}$ of the molecule and the fluorescence intensity $I \propto |\mathbf{p}\cdot\mathbf{E}|^2$ is measured. In this scalar measurement, information about the direction and phase of the polarization vector is lost. The amplitude and phase of an optical near-field can be measured with interferometric near-field techniques,[8,9,11−17] but the directional information is still typically lost. For example, tip-based techniques are mostly sensitive to near fields polarized along the tip axis,[13,15,18−21] making reconstruction of the transverse fields impossible. Phase-dependent transverse near-fields were recently measured with an aperture probe by Burresi et al.,[16] but the reconstruction made explicit use of prior knowledge of the field distribution, namely the absence of normal fields.

In general, optical near fields can be measured only indirectly through the interaction between a probe and sample. This interaction has two limiting regimes: the weak- and strong-tip regimes.[22,23] In the former, the tip is used to map the sample's near field.[23] Since an elongated metal tip is only sensitive to fields polarized along the tip axis, interpretation of images is straightforward, but directional information about polarization is lost. In the latter regime, a strongly interacting tip establishes a locally enhanced field. In this case, the fields must be inferred from the interaction measurements. Without any a priori knowledge about the sample at hand, the reconstruction process is extremely challenging.

In this paper, we study a case in which the probe and sample are equally strong. We use a single gold nanoparticle as a local probe to characterize the near field interaction between the probe and sample. The nanoparticle can be described by a simple dipole model and provides an isotropic polarization response. With a combination of waveplates and polarizers, we can control the polarization of the incident and detected light. Amplitude and phase of the complex field are detected by phase-shifting interferometry.[20] We image a sample consisting of a single gold nanoparticle and show that in this case of two dipoles, the recorded signals correspond to elements of the Green's function tensor that couples the probe and the sample.

A sketch of the experimental situation is shown in Figure 1, along with typical images obtained from scanning gold particles. Polarizers in the excitation and detection path determine whether P or S polarization is detected. The included images are scans of 100 nm gold particles in the case of P-polarized incident and detected light (b) and the case of S-polarized incident light and P-polarized detected light (c). We can immediately see that the polarization combinations correspond to characteristic patterns with the latter exhibiting a double-

* To whom correspondence should be addressed. Telephone: (585) 275-5767. Fax: (585) 276-2112. E-mail: novotny@optics.rochester.edu.

Received for review: 11/9/2009
Published on Web: 01/07/2010

DOI: 10.1021/nl9037505 | *Nano Lett.* **2010,** *10,* 652-656

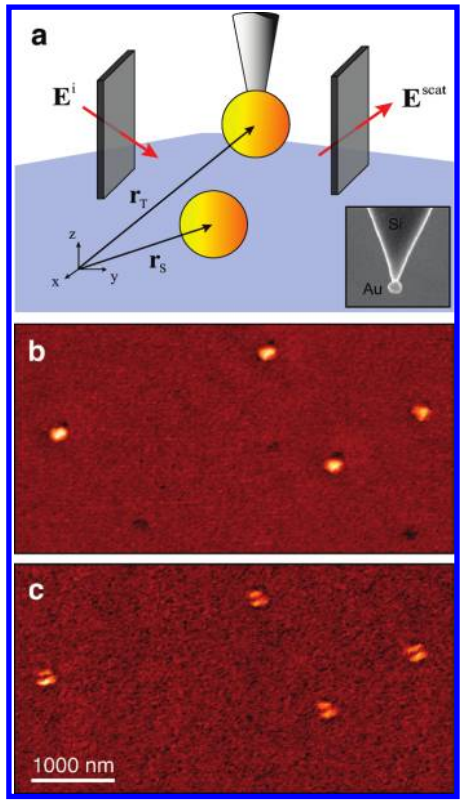

FIGURE 1. (a) Configuration of the experiment. A single gold nanoparticle supported by a silicon tip is used as a local probe. The sample consists of isolated gold nanoparticles. Polarizers in the excitation and detection path control the polarization state of the incident field $\mathbf{E}^i$ and the detected scattered field $\mathbf{E}^{scat}$. Inset: Electron micrograph of a 100 nm gold nanoparticle probe. (b,c) Amplitudes of the detected field recorded by raster-scanning the probe particle over the sample surface. In b, the incident and detected fields are both P-polarized (PP), whereas in c the incident field is S-polarized and the detected field is P-polarized (SP). The different polarizer settings make it possible to extract different elements from the interaction tensor.

lobe pattern. To interpret these images further, we must consider the probe−sample interaction.

The probe-sample region is illuminated with a field $\mathbf{E}^i$ (Figure 1a), which interacts with the probe and sample, and is then scattered away and collected interferometrically as shown in Figure 2. The probe-sample distance is modulated at the frequency Ω, and the detected signal is demodulated at 2Ω. This has the effect of suppressing signals that vary slowly in probe-sample separation, usually defined as background.[24] Since it is necessary to decouple amplitude and phase measured in the interferometric signal, we use phase-shifting interferometry (PSI).[20] At each image pixel, the reference mirror is translated in incremental steps Δx_i from a start position to an end position. Each step Δx_i gives rise to a phase offset δ_i, allowing the interferometric signal at each mirror position (denoted by subscript i) to be written

$$I_i = A + R\cos(\phi + \delta_i) \quad (1)$$

where A is a noninterferometric offset, R is proportional to the amplitude of the scattered field, and ϕ is the phase of the scattered field relative to a constant. A least-squares fitting algorithm then determines A, R, and ϕ for each pixel. In practice, $A \approx 0$ after demodulation.

The polarizers and waveplates in Figure 2 control the incident and reference polarizations. Light from an 831 nm diode laser passes through a half-wave plate and then through a linear polarizer, allowing rotation of linear polarization incident on the sample. A quarter-wave plate in the reference arm rotates the reference polarization when double-passed. Finally, the combined beams pass through a linear polarizer, which selects the polarization of the measured signal. With these elements, combinations of incident and scattered fields from the probe-sample region, notably P and S polarization, are analyzed. The experiment is only weakly sensitive to the angle of the waveplates, which control the light intensity transmitted by the polarizers.

While metal-coated Si tips are typically used as near-field probes because of their large scattering cross-section along the tip axis, we here use a 100 nm gold nanoparticle attached to the end of a Si tip. This provides two advantages: the ability to control the polarization and a simple interaction mechanism between probe and sample. Because of the spherical particle geometry, the probe interacts with the local field isotropically, allowing it to scatter energy from both S and P polarizations, thus providing access to tensorial information about the near field. The probe can be modeled as a dipole, simplifying the interaction between probe and sample and allowing straightforward interpretation of the interaction.

To fabricate the gold nanoparticle probes, standard Si AFM tips are first plasma-cleaned and then placed in a container with the silane APTMS and heated for one hour at 60−80 °C. This functionalizes the silicon so that gold

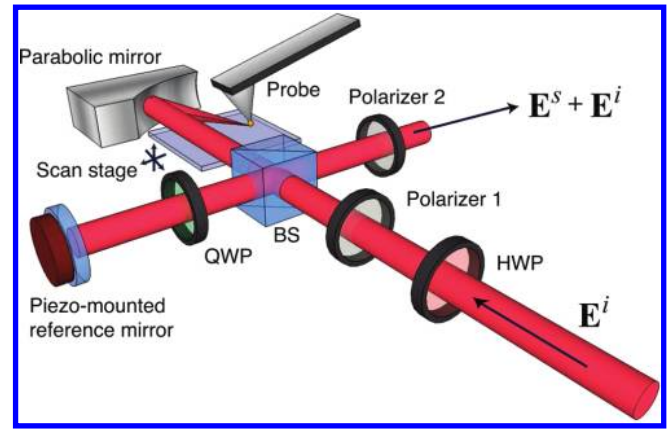

FIGURE 2. Schematic of the experimental setup, consisting of an atomic force microscope and a phase-shifting Michelson interferometer, where a combination of waveplates and polarizers allow control of incident and detected polarizations. The half wave plate and polarizer 1 select the incident polarization, while the quarter wave plate and polarizer 2 select the detected polarization. At each pixel, the piezo-mounted reference mirror is translated, resulting in several measurements with different phase offsets. From this, the amplitude and phase of the signal are determined.

DOI: 10.1021/nl9037505 | *Nano Lett.* **2010,** *10,* 652-656

particles can be attached. A dense sample of 100 nm Au particles is then scanned, and the tip is "pressed" onto the selected particle using the AFM control electronics.

During a scan, the incident and scattered fields are analyzed with polarizers set to either S polarization or P polarization. This renders four distinct polarization measurements, namely SS, SP, PS, and PP (first index refers to incident light and second index to scattered light). The background cannot be fully eliminated by demodulation at 2Ω, but the remainder can be subtracted in postprocessing under the assumption that is nearly constant over the scan region. It is important to note that such subtraction must be done in the complex plane to avoid erroneous results, and thus requires the ability to measure amplitude and phase independently. We note that the background is in general unrelated to the noninterferometric offset A from eq 1, but instead manifests in the measurement of R and ϕ.

The field scattered from the probe-sample region ($\mathbf{E}^{\text{scat}}$ in Figure 1a) is a superposition of fields scattered from the probe and sample. It has been shown that this field can be generally represented by[22]

$$\mathbf{E}^{\text{scat}} = \sum_{n=1}^{\infty} (\mathbf{S} + \mathbf{T})^n \cdot \mathbf{E}^i \tag{2}$$

where the index n denotes the scattering order and $\mathbf{T}$ and $\mathbf{S}$ operate on the incident field, $\mathbf{E}^i$. They represent single scattering events from the probe (T) and sample (S) and are defined by

$$\mathbf{S} \cdot \mathbf{E}(\mathbf{r}_2) \equiv \mathbf{k}_0^2 \int \mathbf{G}(\mathbf{r}_2, \mathbf{r}_1)\eta(\mathbf{r}_1) \cdot \mathbf{E}(\mathbf{r}_1) d^3 r_1 \tag{3}$$

$$\mathbf{T} \cdot \mathbf{E}(\mathbf{r}_2) \equiv \mathbf{k}_0^2 \int \mathbf{G}(\mathbf{r}_2, \mathbf{r}_1)\chi(\mathbf{r}_1) \cdot \mathbf{E}(\mathbf{r}_1) d^3 r_1, \tag{4}$$

where $\mathbf{k}_0$ is the incident free-space wave vector and $\eta(\mathbf{r})$ and $\chi(\mathbf{r})$ are the spatially dependent dielectric susceptibilities of the sample and probe, respectively. $\mathbf{G}(\mathbf{r}_2, \mathbf{r}_1)$ is the dyadic Green's function between the points $\mathbf{r}_1$ and $\mathbf{r}_2$ and is indirectly defined by the field $\mathbf{E}(\mathbf{r}_2)$ radiated by a dipole $\mathbf{p}$ located at $\mathbf{r}_1$ according to[25]

$$\mathbf{E}(\mathbf{r}_2) = \frac{\omega^2}{c^2}\frac{1}{\epsilon_0}\mathbf{G}(\mathbf{r}_2, \mathbf{r}_1)\mathbf{p} \tag{5}$$

The scattering strengths of the probe and sample dictate the number of terms that must be considered from eq 2.

Our experimental situation simplifies eq 2 considerably. The probe and sample are assumed to be identical weakly scattering point dipoles located at $\mathbf{r}_T$ and $\mathbf{r}_S$. Assuming that the scattering series in eq 2 converges, we obtain a first-order approximation by truncating the series to $n \leq 2$, which allows us to represent the detected field as

$$\mathbf{E}^{\text{scat}} = (\mathbf{S} + \mathbf{T} + \mathbf{SS} + \mathbf{TT} + \mathbf{ST} + \mathbf{TS}) \cdot \mathbf{E}^{\text{i}} \tag{6}$$

The quantity in parentheses is the (truncated) optical interaction tensor between the probe and sample, and the incident and detected field polarization states can be used to select combinations of its elements. In tip-based near-field microscopy, the probe is usually taken as a dipole in the direction of the tip axis, so that the polarizability can be approximated as

$$\chi_{\text{tip}}(\mathbf{r}) = \alpha_T \delta(\mathbf{r} - \mathbf{r}_T)\begin{pmatrix} 1 & 0 & 0 \\ 0 & 0 & 0 \\ 0 & 0 & 0 \end{pmatrix} \tag{7}$$

where α_T is the scalar polarizability of the tip. The matrix indicates that the tip is only polarizable along its axis. By contrast, the polarizability of a particle probe is

$$\chi_{\text{tip}}(\mathbf{r}) = \alpha_T \delta(\mathbf{r} - \mathbf{r}_T)\mathbf{I} \tag{8}$$

where $\mathbf{I}$ is the identity tensor. We here investigate the interaction of this tip with an identical particle with polarizability $\eta(\mathbf{r}) = \alpha_S \delta(\mathbf{r} - \mathbf{r}_S)$, where α_S is the sample polarizability. The individual terms of eq 6 can then be written

$$\mathbf{S} = \mathbf{k}_0^2 \alpha_S \mathbf{G}(\mathbf{r}_D, \mathbf{r}_S) \tag{9}$$

$$\mathbf{T} = \mathbf{k}_0^2 \alpha_T \mathbf{G}(\mathbf{r}_D, \mathbf{r}_T) \tag{10}$$

$$\mathbf{SS} = (\mathbf{k}_0^2 \alpha_S)^2 \mathbf{G}(\mathbf{r}_D, \mathbf{r}_S)\mathbf{G}(\mathbf{r}_S, \mathbf{r}_S) \tag{11}$$

$$\mathbf{TT} = (\mathbf{k}_0^2 \alpha_T)^2 \mathbf{G}(\mathbf{r}_D, \mathbf{r}_T)\mathbf{G}(\mathbf{r}_T, \mathbf{r}_T) \tag{12}$$

$$\mathbf{ST} = \mathbf{k}_0^4 \alpha_S \alpha_T \mathbf{G}(\mathbf{r}_D, \mathbf{r}_T)\mathbf{G}(\mathbf{r}_T, \mathbf{r}_S) \tag{13}$$

$$\mathbf{TS} = \mathbf{k}_0^4 \alpha_S \alpha_T \mathbf{G}(\mathbf{r}_D, \mathbf{r}_S)\mathbf{G}(\mathbf{r}_S, \mathbf{r}_T) \tag{14}$$

in which $\mathbf{r}_D$ is the location of the detector. Of the Green's functions in these terms, only $\mathbf{G}(\mathbf{r}_T, \mathbf{r}_S)$ and $\mathbf{G}(\mathbf{r}_S, \mathbf{r}_T)$ vary

DOI: 10.1021/nl9037505 | *Nano Lett.* **2010,** *10,* 652-656

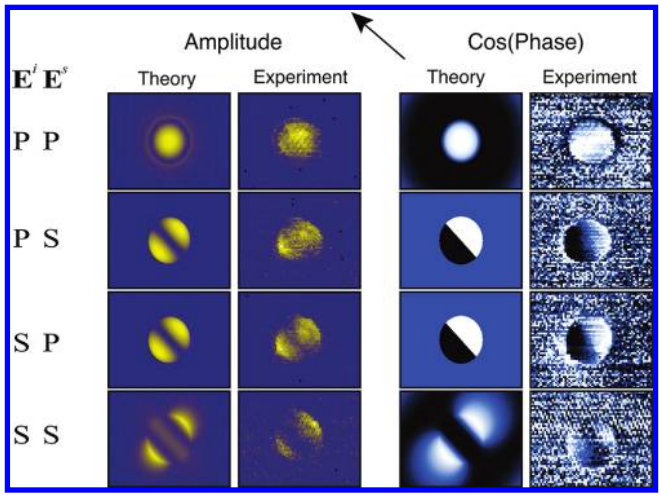

FIGURE 3. Amplitude and phase images of a single 100 nm diameter Au particle for various polarization configurations. According to eq 9, the images correspond to different components of the interaction tensor $\mathbf{G}(\mathbf{r}_2, \mathbf{r}_1)$, where $\mathbf{r}_1$ and $\mathbf{r}_2$ denote the coordinates of the two gold nanoparticles. The arrow indicates the direction of incident light.

substantially with probe−sample distance. Demodulation at the second harmonic of the probe−sample modulation frequency thus suppresses the **S**, **T**, **SS**, and **TT** terms. Since these terms vary slowly in x and y, much of the remaining background can be subtracted in postprocessing.

The **ST** and **TS** terms are further simplified by observing that $\mathbf{G}(\mathbf{r}_D, \mathbf{r}_T) \approx \mathbf{G}(\mathbf{r}_D, \mathbf{r}_S)$ for $\mathbf{r}_D \gg \mathbf{r}_S, \mathbf{r}_T$, and that for a configuration with minimal polarization mixing, they are scalars. Considering that $\mathbf{G}(\mathbf{r}_T, \mathbf{r}_S) = \mathbf{G}(\mathbf{r}_S, \mathbf{r}_T)$ we obtain

$$\mathbf{E}^{scat} \approx 2\mathbf{k}_0^4 \alpha_S \alpha_T G_{DT} \mathbf{G}(\mathbf{r}_S, \mathbf{r}_T) \cdot \mathbf{E}^i \qquad (15)$$

where we have defined the constant G_{DT} to be the scalar version of the Green's function $\mathbf{G}(\mathbf{r}_D, \mathbf{r}_T)$. We note that the quantity $\alpha_S\alpha_T$ factors out, making $\mathbf{E}^{scat}$ sensitive only to their product and not to the relative strength of the polarizabilities. It is clear from eq 9 that elements of the Green's function tensor can be experimentally determined by polarization measurements of incident and scattered fields.

Figure 3 shows the amplitude and phase images for all four combinations of incident and detected polarizations along with corresponding images of the Green's function tensor elements. In our experiments, the probe follows the topography and therefore the surface profile (gold particle) has to be taken into account in the theoretical model. Since the absolute phase offset is arbitrary for each scan, we have added a global phase to each image in order to match it with the theoretical predictions.

Several qualitative features of the experimental and simulated data are evident. In the PP case, a bright center and a faint ring are visible in the amplitude image, and the phase is nearly constant across the particle. The experimental SP and PS cases are similar and identical in theory. They show two bright lobes in amplitude, but the scans exhibit an asymmetry in their brightness, most likely due to slight mixing of the S and P polarization states by the parabolic mirror. Such a mixing would cause the dipoles of probe and sample to be slightly misaligned with the scan plane.

Though two bright lobes are seen in all amplitude patterns except PP, the phase images clearly distinguish between the SP/PS cases and the SS case. There is a sharp jump of ∼180° in the SP and PS phases. The SS phase has a complicated pattern, and the associated low signal makes a comparison difficult, but the two characteristic bright lobes are present on the particle, along with a dark central stripe. The noise in the phase images is due to the vanishing field strength for larger particle−particle separations. Having experimentally determined $\mathbf{G}(\mathbf{r}_S, \mathbf{r}_T)$ we can evaluate the field **E** due to scattering of an arbitrary field $\mathbf{E}_0$ at the sample by $\mathbf{E} \propto \mathbf{G}(\mathbf{r}_S, \mathbf{r}_T)\,\mathbf{E}_0$

It is interesting to note the effect of truncating the series in eq 2. Since the scattering series is geometric, calculating the sum of all interaction terms is straightforward.[26] Included in Figure 3 are theoretical images of the scattered amplitude for each polarization case, taking all terms $n \geq 2$ into account. The PP is similar to the $n = 2$ image, but the ring has faded away. Besides a scaling constant, the SP and PS cases look identical to the $n = 2$ images. In the SS case, the bright stripe in the middle of the $n = 2$ case fades away, which seems to match the experimental data better than the truncated series.

We have chosen two gold nanoparticles as a simple system in which tensorial information about amplitude and phase is important and easily distinguished. In addition to this, the gold nanoparticle dimer system has applications in optical sensing,[27] optical antennas,[28] surface-enhanced Raman scattering,[29] nonlinear optics,[30,31] and molecular rulers,[32,33] for which the interaction tensor between the particles is of interest. As opposed to standard tip-based near field microscopy, our nanoparticle approach makes it possible to retrieve all relevant components of the interaction tensor. The reason tip-based microscopy is not suitable for complete vectorial field mapping is the highly anisotropic polarizability of a tip.[18] The dominant polarizability component along the tip axis prevents access to the SS term of the interaction tensor. There are, however, also limitations of the nanoparticle approach. First, the illumination and collection directions are not parallel to the surface of the sample. Therefore, P-polarized light is in fact a mixture of horizontal and vertical field components. This effect can be minimized by grazing incidence but it leads to large sample illumination areas. Second, the complete field mapping of samples with arbitrary structures (e.g., particle aggregates) requires tomographic reconstructions,[34] which necessitates measurements from multiple excitation and detection

DOI: 10.1021/nl9037505 | *Nano Lett.* **2010,** *10,* 652-656

directions. For example, our experimental scheme can be extended by introducing sample rotation by arbitrary angles.

In conclusion, polarization sensitivity in near-field optics provides insight into the tensor nature of the probe-sample interaction, and in special cases helps to isolate individual Green's function elements. This additional degree of freedom, along with well-defined probe geometries such as gold nanoparticles used in this work are additional tools for fundamental investigation of plasmonic and photonic systems.

Acknowledgment. We thank Palash Bharadwaj and Christiane Hoeppener for help with particle attachment. This work was supported by the National Science Foundation (grant ECCS-0651079).

REFERENCES AND NOTES

(1) Carminati, R.; Greffet, J. J. *Phys. Rev. Lett.* **1999**, *82*, 1660–1663.
(2) Tervo, J.; Setala, T.; Friberg, A. *Opt. Express* **2003**, *11*, 1137–1143.
(3) Wolf, E. *Introduction to the Theory of Coherence and Polarization of Light*, 1st ed.; Cambridge University Press: Cambridge, 2007.
(4) Gersen, H.; Novotny, L.; Kuipers, L.; van Hulst, N. F. *Nat. Photonics* **2007**, *1*, 242.
(5) Lee, K. G.; Kihm, H. W.; Kihm, J. E.; Choi, W. J.; Kim, H.; Ropers, C.; Park, D. J.; Yoon, Y. C.; Choi, S. B.; Woo, D. H.; Kim, J.; Lee, B.; Park, Q. H.; Lienau, C.; Kim, D. S. *Nat. Photonics* **2007**, *1*, 53–56.
(6) Sick, B.; Hecht, B.; Novotny, L. *Phys. Rev. Lett.* **2000**, *85*, 4482–4485.
(7) Novotny, L.; Beversluis, M. R.; Youngworth, K. S.; Brown, T. G. *Phys. Rev. Lett.* **2001**, *86*, 5251.
(8) Balistreri, M. L. M.; Korterik, J. P.; Kuipers, L.; van Hulst, N. F. *Phys. Rev. Lett.* **2000**, *85*, 294–297.
(9) Hillenbrand, R.; Keilmann, F. *Phys. Rev. Lett.* **2000**, *85*, 3029–3032.
(10) Bouhelier, A.; Beversluis, M. R.; Novotny, L. *Appl. Phys. Lett.* **2003**, *83*, 5041–5043.
(11) Dändliker, R.; Tortora, P.; L. Vaccaro, L.; Nesci, A. *J. Opt. A* **2004**, *6*, S18–S23.
(12) Verhagen, E.; Polman, A.; Kuipers, L. *Opt. Express* **2008**, *16*, 45–57.
(13) Kim, D.-S.; Heo, J.; Ahn, S.-H.; Han, S. W.; Yun, W. S.; Kim, Z. H. *Nano Lett.* **2009**, *9*, 3619–3625.
(14) Jones, A. C.; Olmon, R. L.; Skrabalak, S. E.; Wiley, B. J.; Xia, Y. N.; Raschke, M. B. *Nano Lett.* **2009**, *9*, 2553–2558.
(15) Dorfmueller, J.; Vogelgesang, R.; Weitz, R. T.; Rockstuhl, C.; Etrich, C.; Pertsch, T.; Lederer, F.; Kern, K. *Nano Lett.* **2009**, *9*, 2372–2377.
(16) Burresi, M.; Engelen, R. J. P.; Opheij, A.; van Oosten, D.; Mori, D.; Baba, T.; Kuipers, L. *Phys. Rev. Lett.* **2009**, *102*, No. 033902.
(17) Hillenbrand, R.; Keilmann, F.; Hanarp, P.; Sutherland, D. S.; Aizpurua, J. *Appl. Phys. Lett.* **2003**, *83*, 368–370.
(18) Novotny, L.; Stranick, S. J. *Annu. Rev. Phys. Chem.* **2006**, *57*, 303–331.
(19) Gucciardi, P.; Lopes, M.; Deturche, R.; Julien, C.; Barchiesi, D.; de la Chapelle, M. L. *Nanotechnology* **2008**, *19*, 215702.
(20) Deutsch, B.; Hillenbrand, R.; Novotny, L. *Opt. Express* **2008**, *16*, 494–501.
(21) Schnell, M.; Garcia-Etxarri, A.; Huber, A. J.; Crozier, K.; Aizpurua, J.; Hillenbrand, R. *Nature Photon.* **2009**, *3*, 287–291.
(22) Sun, J.; Carney, P. S.; Schotland, J. *J. Appl. Phys.* **2007**, *102*, 103103.
(23) Garcia-Etxarri, A.; Romero, I.; Garcia de Abajo, F. J.; Hillenbrand, R.; Aizpurua, J. *Phys. Rev. B* **2009**, *79*, 125439.
(24) Ocelic, N.; Huber, A.; Hillenbrand, R. *Appl. Phys. Lett.* **2006**, *89*, 101124.
(25) Novotny, L.; Hecht, B. *Principles of Nano-Optics*; Cambridge University Press: Cambridge, 2006.
(26) Novotny, L.; Henkel, C. *Opt. Lett.* **2008**, *33*, 1029–1031.
(27) Enoch, S.; Quidant, R.; Badenes, G. *Opt. Express* **2004**, *12*, 3422.
(28) Bakker, R. M.; Drachev, V. P.; Liu, Z.; Yuan, H.; Rasmus, R. H.; Boltasseva, A.; Chen, J.; Irudayara, J.; Kildishev, A. V.; Shalaev, V. M. *New J. Phys.* **2008**, *10*, 125022.
(29) McMahon, J.; Henry, A.; Wustholz, K.; Natan, M.; Freeman, R.; Duyne, R. V.; Schatz, G. *Anal. Bioanal. Chem.* **2009**, *394*, 1819–1825.
(30) Danckwerts, M.; Novotny, L. *Phys. Rev. Lett.* **2007**, *98*, No. 026104.
(31) Canfield, B. K.; Husu, H.; Laukkanen, J.; Bai, B.; Kuittinen, M.; Turunen, J.; Kauranen, M. *Nano Lett.* **2007**, *7*, 1251–1255.
(32) Sönnichsen, C.; Reinhard, B.; Lipdardt, J.; Alivisatos, A. *Nat. Biotechnol.* **2005**, *23*, 741–745.
(33) Reinhard, B. M.; Siu, M.; Agarway, H.; Alivisatos, A. P.; Lipdardt, J. *Nano Lett.* **2005**, *5*, 2246–2252.
(34) Carney, P. S.; Schotland, J. C. *Appl. Phys. Lett.* **2000**, *77*, 2798–2800.

DOI: 10.1021/nl9037505 | *Nano Lett.* **2010,** *10,* 652-656